The Role of Linear Interference in the Annular Mode Response to Extratropical Surface Forcing

KAREN L. SMITH, CHRISTOPHER G. FLETCHER, AND PAUL J. KUSHNER

Department of Physics, University of Toronto, Toronto, Ontario, Canada

(Manuscript received 30 December 2009, in final form 11 June 2010)

ABSTRACT

The classical problem of predicting the atmospheric circulation response to extratropical surface forcing is revisited in the context of the observed connection between autumnal snow cover anomalies over Siberia and wintertime anomalies of the northern annular mode (NAM). Previous work has shown that in general circulation model (GCM) simulations in which autumnal Siberian snow forcing is prescribed, a vertically propagating Rossby wave train is generated that propagates into the stratosphere, drives dynamical stratospheric warming, and induces a negative NAM response that couples to the troposphere. Important questions remain regarding the dynamics of the response to this surface cooling. It is shown that previously unexplained aspects of the evolution of the response in a comprehensive GCM can be explained by examining the time evolution of the phasing, and hence the linear interference, between the Rossby wave response and the background climatological stationary wave. When the wave response and background wave are in phase, wave activity into the stratosphere is amplified and the zonal-mean stratosphere–troposphere NAM response displays a negative tendency; when they are out of phase, wave activity into the stratosphere is reduced and the NAM response displays a positive tendency. The effects of linear interference are probed further in a simplified GCM, where an imposed lower tropospheric cooling is varied in position, strength, and sign. As in the comprehensive GCM, linear interference strongly influences the response over a realistic range of forcing strengths. The transition from linear to nonlinear behavior is shown to depend simply on forcing strength.

1. Introduction

Predicting the response of low-frequency modes of atmospheric variability such as the North Atlantic Oscillation and the northern annular mode (NAM; Thompson and Wallace 1998, 2000) to extratropical surface anomalies represents a classical challenge in climate science (e.g., Robinson 2000; Kushnir et al. 2006). These modes are intrinsically difficult to predict because they are internally generated by tropospheric eddy-mean flow interactions that are stochastic in character and because they are modulated by multiple influences, including interactions with the ocean surface, the land surface, and the stratosphere (DeWeaver and Nigam 2004; Limpasuvan and Hartmann 2000; Czaja and Frankignoul 2002; Gong et al. 2002; Baldwin et al. 2003). In simulations, the response of the modes to a prescribed forcing is model dependent because many details, including the characteristics of the modes, the temporal and spatial structure of the forcing, the background flow, and model configuration, all appear to matter for the extratropical response to surface forcing. In an attempt to better constrain some aspects of the problem, we here present a straightforward diagnostic approach based on linear interference effects found in the simulated response to a particular extratropical forcing. The approach is only partially predictive and in this study applies mainly to the high-latitude stratospheric circulation response. But it accounts for some previously unexplained and nonrobust aspects of the response, and we find that it applies more broadly to other problems of this class (Fletcher and Kushner 2011).

Our focus is on the dynamical forcing of large-scale circulation anomalies by terrestrial snow cover. While variations in terrestrial snow cover exert a strong radiative, thermal, and hydrological influence on global climate (Cohen and Rind 1991; Groisman et al. 1994; Vavrus 2007; Brown and Mote 2009), recent work has focused on the atmospheric circulation response to snow-related

Corresponding author address: Karen L. Smith, Department of Physics, University of Toronto, 60 St. George Street, Toronto ON M5S 1A7, Canada.
E-mail: ksmith@atmosp.physics.utoronto.ca

DOI: 10.1175/2010JCLI3606.1

shortwave cooling and thermal forcing (e.g., Cohen and Entekhabi 1999; Gong et al. 2003; Fletcher et al. 2009a,b; Sobolowski et al. 2010; Henderson and Leathers 2009). Here we consider the observation that years in which snow cover extent is anomalously large over Eurasia in October tend to be years in which the NAM in the following winter is in its negative phase. A proposed explanation is that positive snow cover extent anomalies generate strong regional surface cooling via increasing surface albedo, which excites a vertically propagating Rossby wave train in late fall and early winter (e.g., Gong et al. 2003; Cohen et al. 2007). The waves are dissipated in the stratosphere, leading to a negative NAM response consisting of a stratospheric warming and downward propagation of a negative NAM signal to the troposphere by January (Baldwin and Dunkerton 2001).

Although GCM studies with prescribed October Siberian snow forcing capture important features of the proposed mechanism (Gong et al. 2003; Fletcher et al. 2009a), questions remain regarding the transient evolution and dynamics of the response. For example, Fletcher et al. (2009a) focused on a downward-propagating negative NAM (weak vortex) response to prescribed snow forcing that corresponds to the observed behavior; however, their simulation also includes an initial weak positive NAM (strong vortex) response that remains unexplained and is not detected in observations. In addition, only partially understood is the mechanism whereby the negative NAM response peaks and decays, despite the fact that the snow forcing remains switched on and a robust upward-propagating Rossby wave train response persists. The unexplained aspects of the Fletcher et al. (2009a) simulations add to outstanding questions regarding the inability of GCMs with predicted (as opposed to prescribed) snow cover to capture the snow–circulation connection (Hardiman et al. 2008).

Our emphasis on linear interference effects is motivated by recent observational and modeling work on the coupled stratosphere–troposphere response to tropospheric forcing. For example, Garfinkel and Hartmann (2008) have shown that ENSO primarily affects the stratospheric polar vortex through a Pacific–North America–like teleconnection pattern that constructively or destructively interferes with the wave 1 quasi-stationary wave field in the troposphere and thus strengthens or weakens the Eliassen–Palm (E–P) flux into the stratosphere. This, in turn, weakens or strengthens the polar vortex via wave-induced stresses on the zonal mean circulation. Besides ENSO-related forcing of climate, Garfinkel et al. (2010) show that Eurasian snow cover anomalies similarly influence the wave 1 quasi-stationary wave field and hence the E–P flux into the stratosphere. Other studies indicate that linear interference effects are at work in stratosphere–troposphere coupling. For example, Martius et al. (2009) show that tropospheric blocking events that are collocated with the climatological wave 1 and wave 2 quasi-stationary wave fields are associated with wave 1 and wave 2 stratospheric sudden warmings, respectively. In addition, Ineson and Scaife (2009) show that the extratropical stratosphere–troposphere response to ENSO in simulations is controlled by the coherence between the ENSO anomaly and the background waves.

In this study, we apply these insights to study linear interference effects in the snow-forced teleconnection to the NAM. Our main point is that the phase of the wave response to the surface forcing relative to the phase of the background stationary wave plays a key role in determining the zonal-mean response to surface cooling. Section 2 outlines the models employed in this study and our experimental design. In section 3a, we will explore details of the transient response to a Siberian snow forcing in a comprehensive GCM simulation. We use a simplified GCM to investigate and diagnose the dynamics in greater detail in sections 3b, 3c, and 3d. Section 4 summarizes our conclusions.

2. Methods

a. Model descriptions

We revisit the simulations performed by Fletcher et al. (2009a, henceforth F09) with the low-top Geophysical Fluid Dynamics Laboratory (GFDL) atmospheric and land GCM AM2–LM2 (Anderson et al. 2004; denoted AM2-LO in F09). Although this model does not have a well-resolved stratospheric circulation, we believe this is not critical in determining the response (F09). The specifics of the model configurations are discussed in detail in F09. Owing to an irrecoverable data loss, the number of ensemble members used in this study is 52 versus the 100 ensemble members used in F09. The ensemble-mean results we consider are unaffected by this change.

We also use a simplified GCM (SGCM) that solves the dry, hydrostatic, primitive equations in hybrid coordinates (Polvani and Kushner 2002; Held and Suarez 1994). It is forced with a Newtonian relaxation of the temperature to a prescribed, zonally symmetric and time-independent, equilibrium temperature profile T_{eq}. The SGCM is not constructed to closely correspond to the comprehensive GCM, AM2, but it will serve to test dynamical ideas (e.g., while AM2 has a seasonal cycle, the SGCM equilibrium temperature profile is independent of time such that the climatology is representative of Northern Hemisphere winter solstice conditions). In this model, the strength of the NAM response to tropospheric

forcings is sensitive to the strength of the polar vortex (Reichler et al. 2005; Gerber and Polvani 2009), which can be adjusted by specifying γ, the temperature lapse rate over the winter pole in the equilibrium temperature profile. We choose $\gamma = 2$ K km^{-1} in this study. The model has 40 vertical levels (model lid height of 0.02 hPa), a horizontal resolution of T42, and is run with a time step of 800 s. Additional details are given in Polvani and Kushner (2002) and Kushner and Polvani (2004). The most important difference from previous studies is that in this study, the SGCM uses realistic topography (i.e., the T42 spectral representation of the observed topographic distribution) instead of idealized topography or no topography, which allows for the generation of a planetary stationary wave field (Fig. 5, shading) with a fairly realistic phase structure. But the amplitude of the resulting stationary wave in the SGCM is too weak compared to observations, and also to the comprehensive GCM, AM2. For example, the amplitude of the climatological stationary wavenumber 1 at 60°N and 50 hPa is 45 m in the SGCM, 141 m in AM2 [December–February (DJF)], and 229 m in National Centers for Environmental Prediction (NCEP) for 1967–2007 (DJF). We will discuss below the consequences the weak stationary wave field has on our SGCM results.

b. Snow/surface cooling method

F09 apply a "switch on" positive snow forcing in the comprehensive GCM, AM2, over the Siberian region for October–December; this increases surface albedo and generates a surface shortwave cooling. F09 branch "high snow" and "low snow" integrations from independent initial states taken from a long "climatological SST" control integration. In these integrations the difference between the snow depth in the high-snow and low-snow cases is time independent. Further details of the snow forcing perturbation method for the comprehensive GCM are provided in Fletcher et al. (2007) and F09. Regarding the low-snow state as the background state or control state c and the high-snow state as the perturbed state, p we define the response in X as

$$\Delta X = X_p - X_c \tag{1}$$

for a given realization. Then, denoting an ensemble mean by angled brackets $\langle\cdot\rangle$, the ensemble-mean response is

$$\Delta\langle X\rangle = \langle X_p\rangle - \langle X_c\rangle. \tag{2}$$

TABLE 1. List of SGCM simulations. Each simulation consists of ninety 100-day ensemble members. A forcing strength of 1 corresponds to the standard forcing strength $Q_0 = -3.125$ K day^{-1} in Eq. (3).

Simulation	Forcing location (λ_1–λ_2) (°)	Forcing strength
A	30–110	1
B	60–140	1
C	90–170	1
D	120–200	1
E	150–230	1
F	180–260	1
G	210–290	1
H	240–320	1
I	270–350	1
J	300–20	1
K	330–50	1
L	0–80	1
M	60–140	0.5
N	60–140	1.5
O	60–140	2
P	60–140	2.5
Q	60–140	3
R	60–140	3.5
S	30–110	−1

The SGCM is used to explore a broad range of surface thermal forcings, including variations in the strength, position, and sign of the forcings. These simulations are listed in Table 1 and the motivation for using them will be presented in sections 3b and 3c. We prescribe lower-tropospheric cooling over a region bounded to the west at longitude λ_1 and to the east at longitude λ_2, and to the south and north by latitudes 40° and 80°N. We add a term, $Q(\lambda, \varphi, \sigma)$, to the temperature tendency equation, where φ is latitude and σ is the vertical sigma coordinate; Q is defined by

$$Q = \begin{cases} 0, & \lambda < \lambda_1, \varphi < 40°\text{N} \\ Q_0(\varphi_0/\varphi)^3 \max\{0, [(\sigma - \sigma_b)/(1 - \sigma_b)]\}, & \lambda_1 \le \lambda \le \lambda_2, 40°\text{N} \le \varphi \le 80°\text{N}, \\ 0, & \lambda > \lambda_2, \varphi > 80°\text{N} \end{cases} \tag{3}$$

where φ_0 is 40°N and Q_0 was chosen to achieve a cooling response that resembled the cooling response to the snow forcing in AM2 ($Q_0 = -3.125$ K day^{-1} gives an area-averaged forcing of -1.4 K day^{-1} at $\sigma = 1$). The forcing is strongest at the surface and decreases linearly to zero in the vertical up to $\sigma_b = 0.7$ and decreases meridionally as φ^{-3} from 40° to 80°N to mimic the effect of the decreasing meridional insolation gradient on

snow-related shortwave diabatic cooling in fall and winter. For a Siberian forcing, corresponding to F09, $\lambda_1 = 60°E$ and $\lambda_2 = 140°E$. We have run similar simulations using other forcing shapes—for example, two-dimensional sine-squared forcings centered at 60°N and 100°E—and find that our results are qualitatively similar. In addition to the simulations run with the forcing centered over Siberia (simulation B in Table 1; see section 3b), we have also run 11 additional simulations (simulations A and C–L) in which the forcing is shifted zonally at intervals of 30° longitude [i.e., λ_1 and λ_2 in (3) are increased in 30° increments], another series of simulations in which the strength of the forcing over Siberia is varied (simulations M–R), and one additional simulation in which the applied forcing was a heating rather than a cooling (simulation S).

For all SGCM perturbation simulations, a 9000-day control run with time-independent forcing is used to provide initial conditions for ninety 100-day realizations. The forcing is switched on and held constant for 100 days. For these simulations, the response is given by Eqs. (1) and (2), with p referring to the forced state and c referring to the corresponding control state.

3. Results

a. Revisiting the transient response to Siberian snow forcing in F09

Figure 1a shows the ensemble-mean time series of the 60°–90°N polar-cap-averaged 50-hPa geopotential height (GPH) response $\Delta\langle Z_{\mathrm{pcap}}\rangle$ to snow forcing in AM2. Anomalous polar cap geopotential Z_{pcap} is a proxy for the NAM index (Baldwin and Thompson 2009), a positive ΔZ_{pcap} corresponds to a negative NAM response and vice versa. Fletcher et al. (2007) and F09 discuss the vertical structure of this response, its downward propagation in the stratosphere, and its coupling to the troposphere; the 50-hPa response is a good proxy for the lower-stratospheric response as a whole. Over the first 15 days of the simulation, there is a slight decrease in $\Delta\langle Z_{\mathrm{pcap}}\rangle$, followed by a linear increase until day 65, and a sharp drop off afterward. We identify two distinct periods of evolution: the time interval before the peak in $\Delta\langle Z_{\mathrm{pcap}}\rangle$ in Fig. 1a (days 1–65), which is characterized by an overall negative NAM tendency, and the time interval after the peak in $\Delta\langle Z_{\mathrm{pcap}}\rangle$ (days 66–92), which is characterized by a positive NAM tendency (we will return to the issue of the weak positive NAM feature during the first 15 days of the transient simulation below).

Figures 1b,c show the ensemble-mean longitude-level cross section of the wave response $\Delta\langle Z^*\rangle$ at 60°N averaged over days 1–65 and days 66–92, respectively. Here, the asterisk superscript, $(\cdot)^*$, indicates the deviation from the zonal mean. The wave response at 60°N is representative of the high extratropical wave response in the latitude band 50°–70°N. During both periods, we observe a characteristic westward-tilting wave structure associated with upward-propagating Rossby waves originating from the forcing region. At first, this seemed to imply to us that snow forcing was consistently associated with a positive net upward wave activity response. But the GPH tendency in Fig. 1a is positive in the first period and negative in the second period. Consistently, when we calculate the response of the ensemble-, time-, and zonal-mean meridional eddy heat flux, which is a proxy for the vertical component of the E–P flux (Newman et al. 2001; Polvani and Waugh 2004), we see an increase in the eddy heat flux during the day 1–65 period (Fig. 2a) and a decrease of the eddy heat flux during the day 66–92 period (Fig. 2d). The change in the sign of the $\Delta\langle Z_{\mathrm{pcap}}\rangle$ tendency during the simulation corresponds to the change in sign of the eddy heat flux response in an analogous manner to that observed during natural negative and positive NAM events (McDaniel and Black 2005). Thus, our original inference about the change in wave activity, based on examining the eddy GPH response alone, is incorrect.

To explain the change in sign of the wave activity response between the two periods, we need to consider the nonlinear nature of the eddy heat flux response. We denote the ensemble-mean eddy heat flux response as $\Delta\{\langle v^*T^*\rangle\}$, where the braces, $\{\cdot\}$, indicates zonal and time averaging. For each ensemble member, we define

$$v^* = \langle v^*\rangle + v^{*\prime}, \quad T^* = \langle T^*\rangle + T^{*\prime}, \tag{4}$$

where the prime superscript, $(\cdot)'$, denotes the departure from the ensemble mean. The ensemble-mean eddy heat flux response can then be decomposed as

$$\Delta\{\langle v^*T^*\rangle\} = \Delta\{\langle v^*\rangle\langle T^*\rangle\} + \Delta\{\langle v^{*\prime}T^{*\prime}\rangle\}. \tag{5}$$

We call the first term on the right-hand side of (5) "EM," as it characterizes the contributions from the ensemble-mean response, and we call the second term "FL," as it characterizes the contributions from the fluctuations about the ensemble mean. Thus, we can write

$$\Delta\{\langle v^*T^*\rangle\} = \mathrm{TOTAL} = \mathrm{EM} + \mathrm{FL}, \tag{6}$$

where

$$\mathrm{EM} \equiv \Delta\{\langle v^*\rangle\langle T^*\rangle\} \quad \text{and} \quad \mathrm{FL} \equiv \Delta\{\langle v^{*\prime}T^{*\prime}\rangle\}.$$

We find, and will shortly confirm, that TOTAL is dominated by EM, that is, $\Delta\{\langle v^*T^*\rangle\} \approx \Delta\{\langle v^*\rangle\langle T^*\rangle\}$. The

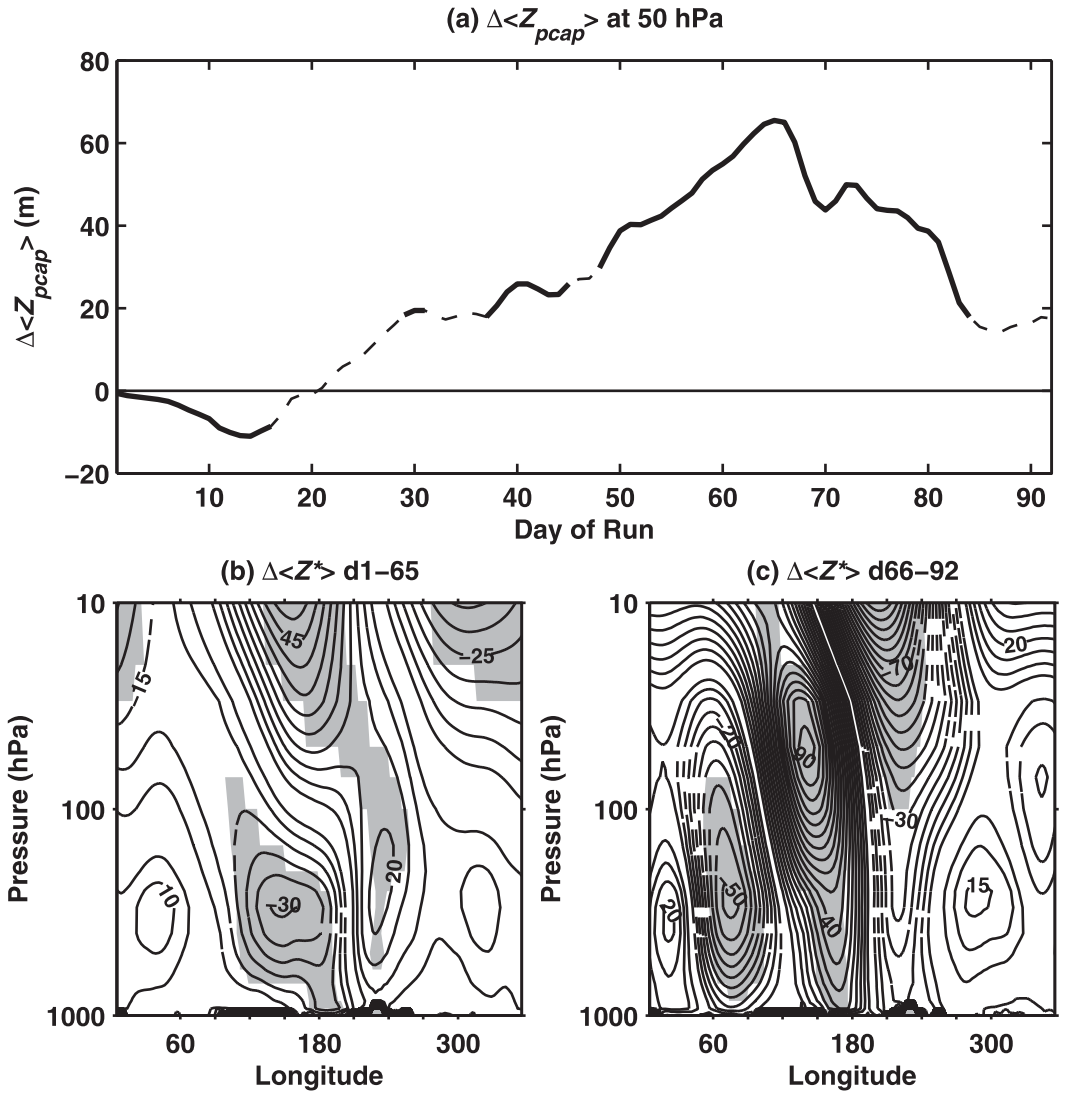

FIG. 1. (a) Time series of $\Delta\langle Z_{\mathrm{pcap}}\rangle$ to a switch-on snow forcing in the AM2 GCM. Thick, solid portions of the line indicate 95% significance (the statistical significance of the response is assessed for each simulation day using the 1-sample Student's *t* test, assuming independence of the realizations that start 1 yr apart). The solid horizontal line indicates the 0 line. (b) Days 1–65 averaged ensemble mean eddy GPH response ($\Delta\langle Z^*\rangle$) at 60°N. (c) As in (b), but for days 66–92. The solid (dashed) contours correspond to positive (negative) values. The contour interval is 5 m. The gray shading shows 95% significance.

ensemble averaging effectively low-pass filters the dynamics and so the EM term represents contributions to the response from relatively low-frequency waves. The FL term is small here and is dominated by contributions from relatively high-frequency waves—for example, synoptic waves in the troposphere—that are independent in each realization but contribute systematically to the eddy fluxes from one realization to the next.

The response of the EM eddy heat flux can be decomposed straightforwardly into terms that are linear and quadratic in the ensemble-mean response. Using Eq. (1), we have

$$\mathrm{EM} = \mathrm{EM}_{\mathrm{LIN}} + \mathrm{EM}_{\mathrm{NL}}, \tag{7}$$

where

$$\mathrm{EM}_{\mathrm{LIN}} = \left\{\langle v_c^*\rangle \Delta\langle T^*\rangle + \Delta\langle v^*\rangle\langle T_c^*\rangle\right\} \quad \text{and}$$
$$\mathrm{EM}_{\mathrm{NL}} = \{\Delta\langle v^*\rangle \Delta\langle T^*\rangle\}.$$

The term $\mathrm{EM}_{\mathrm{LIN}}$ represents the eddy heat flux response associated with the covariance (under a time and zonal mean, $\{\cdot\}$) between the ensemble-mean wave response ($\Delta\langle v^*\rangle$ and $\Delta\langle T^*\rangle$) and the control state ($\langle v_c^*\rangle$ and $\langle T_c^*\rangle$). The term $\mathrm{EM}_{\mathrm{LIN}}$ is *linear* in the ensemble-mean wave

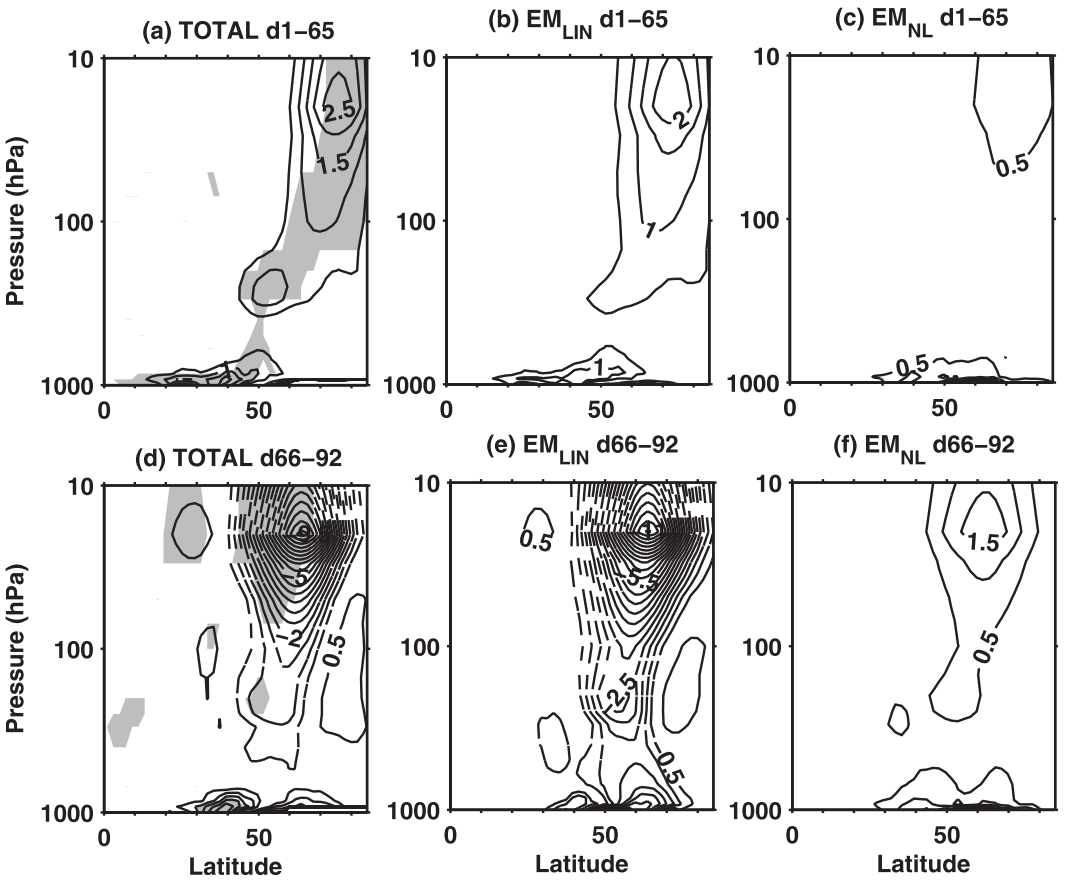

FIG. 2. (a) Days 1–65 averaged $\Delta\{\langle \nu^* T^* \rangle\}$. (b) The EM_{LIN} contribution to $\Delta\{\langle \nu^* \rangle \langle T^* \rangle\}$. (c) The EM_{NL} contribution to $\Delta\{\langle \nu^* \rangle \langle T^* \rangle\}$. (d)–(f) As in (a)–(c), but for days 66–92. The contour interval is 0.5 m K s^{-1}. For (a), the Student's t test is computed using the time-averaged fields; the gray shading shows 95% significance. We have found it difficult to derive straightforward significance tests for the EM_{LIN} and EM_{NL} terms that are consistent with the t test on $\Delta\{\langle \nu^* T^* \rangle\}$. Thus, significance shading is not included in (b),(c),(e), and (f); however, we have verified that the main features are robust by subsampling the ensemble.

response—for example, EM_{LIN} would double if the amplitude of the wave response doubled. The term EM_{NL} involves only the ensemble-mean wave response and thus represents the eddy heat flux response intrinsic to the wave response itself. The term EM_{NL} is *quadratic* in the ensemble-mean wave response—for example, EM_{NL} would quadruple if the amplitude of the wave response doubled.

TOTAL, EM_{LIN}, and EM_{NL} are plotted in Figs. 2a–c for the day 1–65 period and in Figs. 2d–f for the day 66–92 period. In both periods, TOTAL, that is $\Delta\{\langle \nu^* T^* \rangle\}$, is seen to be dominated by EM_{LIN}; EM_{NL} is relatively small. Figure 2 also confirms that $\Delta\{\langle \nu^* T^* \rangle\} \approx \Delta\{\langle \nu^* \rangle \langle T^* \rangle\}$, which itself represents a considerable simplification (we have separately verified that $\Delta\{\langle \nu^* T^* \rangle\} - \Delta\{\langle \nu^* \rangle \langle T^* \rangle\}$ is generally small throughout the integration). The key point arising from Fig. 2 is that the EM_{LIN} term changes sign from positive to negative in the stratosphere from the first to the second period and thereby accounts for the switch in sign of $\Delta\{\langle \nu^* T^* \rangle\}$. We will see that the switch in sign comes about because the wave response reinforces the control state wave in the first period and attenuates the control state wave in the second period. In other words, the response at first constructively interferes with the control state wave and then destructively interferes with it. The EM_{NL} term, on the other hand, is smaller but remains positive for both periods, consistent with the upward-propagating wave energy inferred from Figs. 1b,c. Here EM_{NL} is small primarily because the wave response amplitude is small compared to the control state wave (see section 3c). Thus, the change in sign of the wave activity between the two periods, and hence the change in the sign of the tendency of the zonal-mean response, is controlled by linear interference effects.

To more clearly demonstrate the interference effect, it is useful to compare the relative phase of the wave response and the control state wave over time. We focus

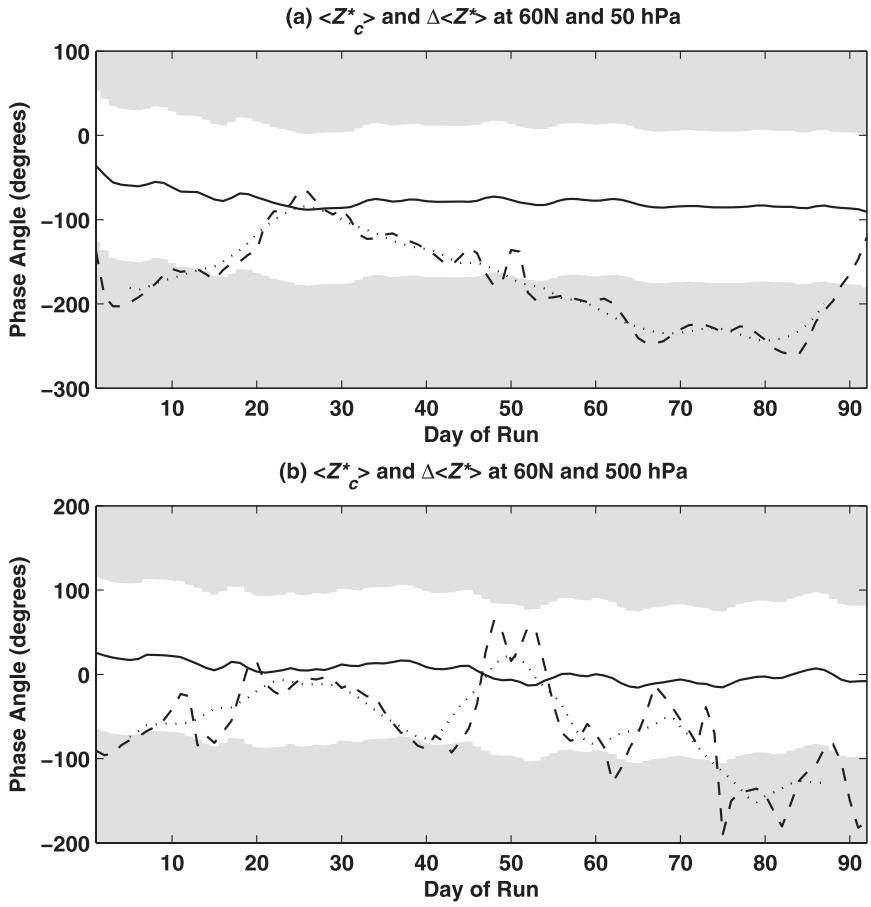

FIG. 3. Time series of 60°N wave 1 phase in degrees for $\langle Z_c^* \rangle$ (solid line) and for $\Delta\langle Z^* \rangle$ with (dotted line) and without (dashed line) a 10-day running mean applied at (a) 50 and (b) 500 hPa. The gray shading indicates regions where $\langle Z_c^* \rangle$ and $\Delta\langle Z^* \rangle$ are out of phase.

on the wave 1 component, since this controls the overall character of the response. Figure 3 shows the time series of the phase of the wave 1 eddy GPH (i.e., the longitude of the positive eddy GPH anomaly) for the control state wave $\langle Z_c^* \rangle$ and for the ensemble-mean response $\Delta\langle Z^* \rangle$ at 60°N and 50 hPa (Fig. 3a) and at 60°N and 500 hPa (Fig. 3b). The time series with a 10-day running mean applied is also shown. In the stratosphere, $\Delta\langle Z^* \rangle$ starts roughly 105° out of phase with $\langle Z_c^* \rangle$ at the outset of the simulation and rapidly shifts 65° further out of phase (westward) over the first few days. This results in destructive interference and a suppression of the wave activity flux into the stratosphere up to approximately day 19 (not shown) and accounts for the weak positive NAM feature observed during the first 20 days of the simulation (Fig. 1a). As the simulation progresses through the first 65 days, $\Delta\langle Z^* \rangle$ shifts eastward until roughly day 26 in both the troposphere and the stratosphere and becomes relatively in phase with $\langle Z_c^* \rangle$. After day 26, the phase of $\Delta\langle Z^* \rangle$ is more variable in the troposphere, reflecting greater synoptic variability in this region; however, $\Delta\langle Z^* \rangle$ clearly shifts westward in the stratosphere and becomes relatively out of phase with $\langle Z_c^* \rangle$ during days 66–92.

We note that we saw the east–west shifting of the wave response in F09 but did not appreciate its significance in that study. We will examine the robustness of these linear interference effects in the SGCM in the next subsection.

b. Comparison between AM2 and the SGCM

We test dynamical ideas about the snow–NAM teleconnection by conducting idealized perturbation simulations in the SGCM. The initial regional response to the imposed Siberian lower tropospheric cooling in the SGCM (henceforth the ''Siberian case,'' which corresponds to simulation B in Table 1) bears some similarity to that in AM2. As in AM2, the direct response to the forcing is a surface cooling localized over the forcing region. The ensemble-mean surface cooling over the forcing region stabilizes at approximately −5.5 K by day 30.

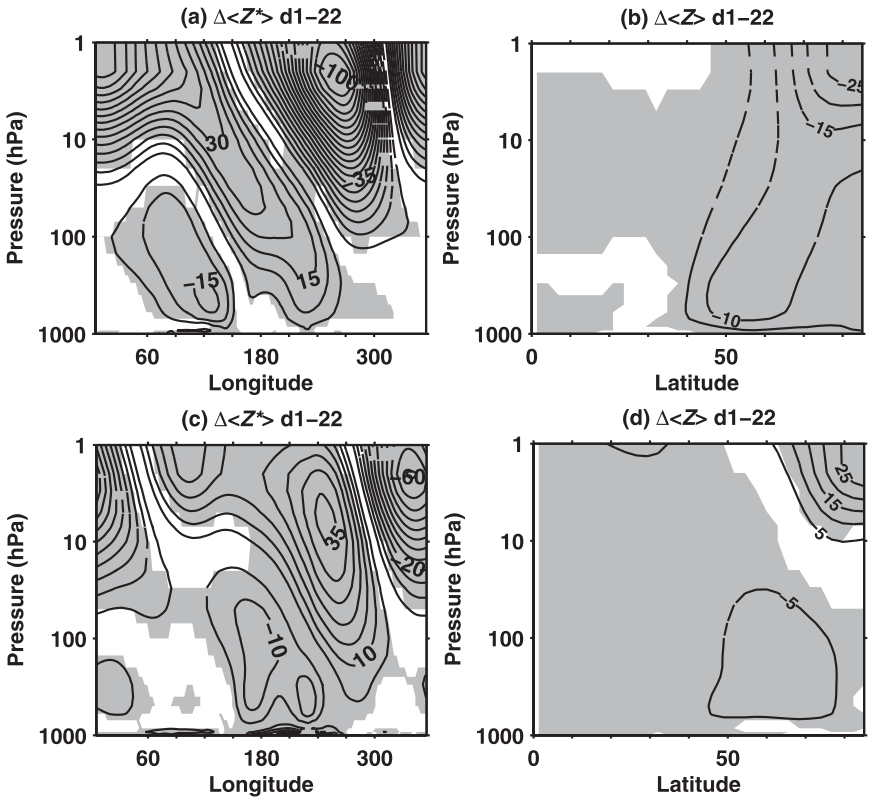

FIG. 4. Days 1–22 averaged ensemble mean response to Siberian lower-tropospheric cooling in the SGCM: (a) $\Delta\langle Z^*\rangle$ at 60°N and (b) $\Delta\langle Z\rangle$. (c),(d) As in (a) and (b), but for the Pacific lower-tropospheric cooling case. The solid (dashed) contours correspond to positive (negative) values, and the gray shading shows 95% significance. The contour interval is 5 m.

This is approximately 2 K cooler than the surface cooling observed in F09, but this discrepancy is not qualitatively important for our analysis (see section 3d). Over the first several weeks, a local surface high in sea level pressure (SLP) and a deep upper-level low in GPH extending to the upper troposphere develop over the forcing region in the SGCM simulation (not shown), which are broadly consistent with F09. Despite these similarities with AM2, the hemispheric zonal-mean response is significantly different.

Figure 4a shows the ensemble-mean longitude-level cross section of $\Delta\langle Z^*\rangle$ at 60°N averaged over days 1–22. The SGCM Rossby wave response is quite coherent and has a more pronounced westward tilt with height than the AM2 wave response (Fig. 1b). Seeing this, we at first anticipated a similar or stronger negative NAM response to the forcing in the SGCM. But for this case, we obtain a negative-signed zonal-mean GPH response that corresponds to a *positive* NAM response. The zonal-mean GPH response $\Delta\langle Z\rangle$ for days 1–22 is shown in Fig. 4b. This positive NAM response develops early and retains the same sign throughout the 100-day simulation; however, it is not significant beyond day 22 (not shown). Unlike the AM2 case, there are no reversals of sign of the GPH tendency. The positive NAM response is inconsistent with the dominant negative NAM response in AM2, with observational results (Cohen and Entekhabi 1999; Cohen et al. 2007; Hardiman et al. 2008) and with other modeling studies (Gong et al. 2003).

Besides the difference in sign, there are other quantitative differences between the AM2 and SGCM response. First, the SGCM stratospheric NAM response is relatively confined to the mid-to-upper stratosphere, whereas the AM2 stratospheric NAM response extends into the lower stratosphere (F09). The reduced SGCM response in the lower stratosphere is consistent with the generally weak stratosphere–troposphere coupling in the SGCM, which is particularly sensitive to the choice of equilibrium temperature profile and topographic configuration (Gerber and Polvani 2009; Chan and Plumb 2009). Second, the AM2 response, which remains significant up to days 60–90, is more persistent than the SGCM response, which is only significant up to day 22. Our level of understanding of this behavior is poor, given that the persistence of annular mode signals is generally biased high (Gerber et al. 2008a) and is strongly model dependent

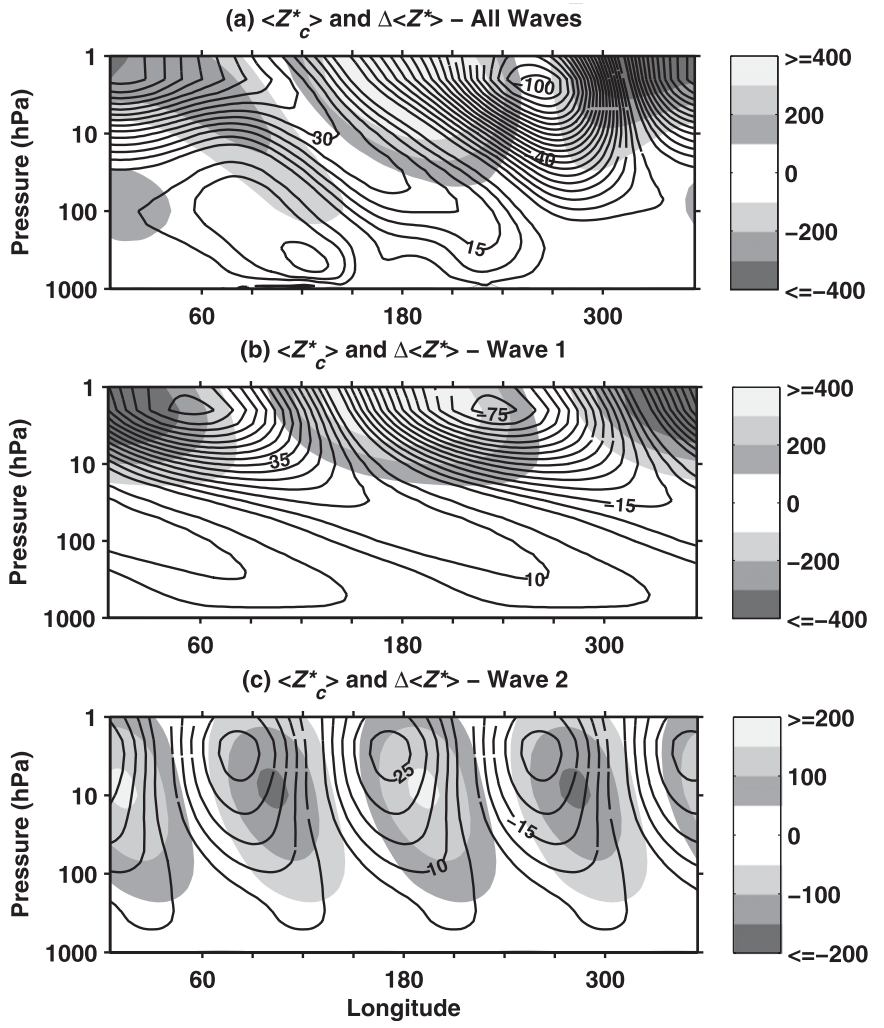

FIG. 5. Days 1–22 averaged $\Delta\langle Z^*\rangle$ (black contours) at 60°N to Siberian lower-tropospheric cooling in the SGCM superimposed on $\langle Z_c^*\rangle$ at 60°N (gray shading) for (a) all waves, (b) wave 1, and (c) wave 2. The contour interval is 5 m.

(Gerber et al. 2008b). Related to the current study, in F09, a version of AM2 with enhanced stratospheric resolution also showed a much less persistent response to snow forcing than the standard AM2 used here. We will not be able to further address the important differences between the simplified and comprehensive GCMs within this study; however, we point out that there are several potential dynamical controls, many of which were discussed in F09 and Hardiman et al. (2008), that need to be considered.

Our main aim in the remainder of this analysis will be to answer the more focused question of what controls the *sign* of the NAM response; this can be understood more clearly when we investigate the role of linear interference in the SGCM simulations. We find it instructive to compare the wave structure of the response and the control state in detail to assess linear interference effects. Figure 5a again plots days 1–22 $\Delta\langle Z^*\rangle$ at 60°N (as in Fig. 4a) but this time superimposed on $\langle Z_c^*\rangle$. Figures 5b,c show the wave 1 and wave 2 components of both fields. We find that the log-pressure-weighted spatial correlation of $\Delta\langle Z^*\rangle$ and $\langle Z_c^*\rangle$ is -0.36 for the all-wave response (indicating destructive interference), -0.55 for the wave 1 component (destructive interference), and 0.84 for the wave 2 component (constructive interference). Although the magnitude of the correlation for the wave 1 response is smaller than for the wave 2 response, the sign of the all-wave correlation is determined by the larger-amplitude wave 1 component, particularly in the stratosphere.

As we will demonstrate in our discussion of Fig. 6 below, in the SGCM simulations, as for the AM2 case, the

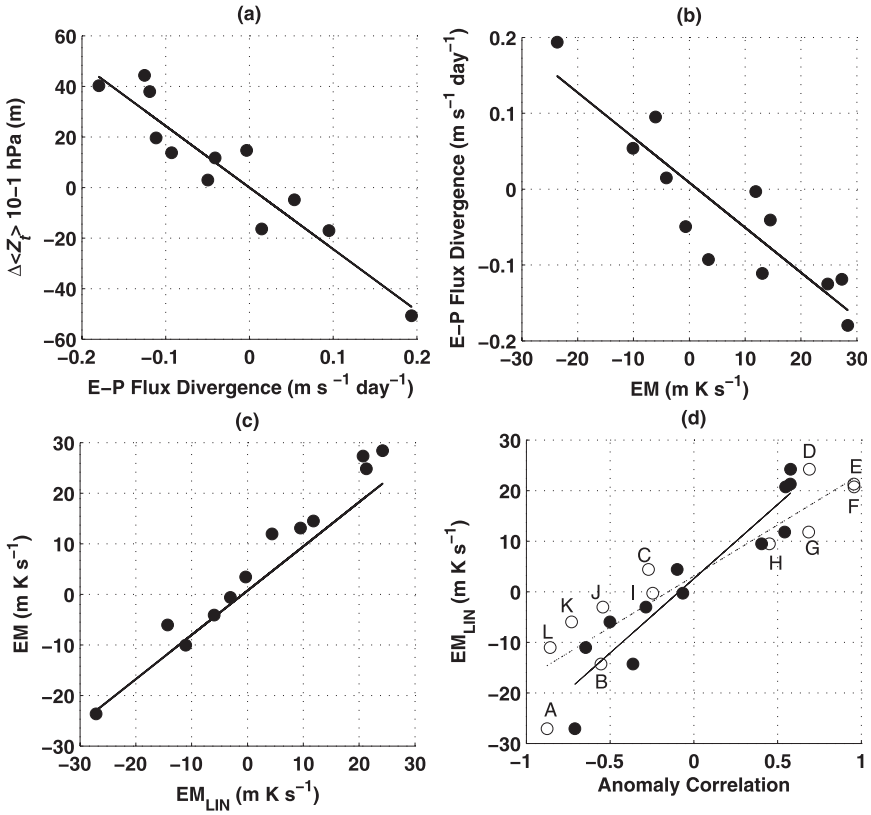

FIG. 6. Dependence of the SGCM response on forcing location (simulations A–L in Table 1). (a) The TOTAL E–P flux divergence response averaged over 40°–80°N, 10–1 hPa, and days 1–22 vs the 10–1-hPa $\Delta\langle Z_t\rangle$ averaged over the polar cap and over days 10–40. (b) $\Delta\{\langle v^*\rangle\langle T^*\rangle\}$ (EM) at 10 hPa, averaged over 40°–80°N, and cumulative to day 22 vs the E–P flux divergence response. (c) EM_{LIN} vs EM. (d) The all-wave (solid circles) and wave-1 (open circles) spatial correlation between $\Delta\langle Z^*\rangle$ and $\langle Z_c^*\rangle$ vs EM_{LIN}.

term $\Delta\{\langle v^*\rangle\langle T^*\rangle\}$ (EM) dominates the wave driving response and the EM_{LIN} contribution is larger than the EM_{NL} contribution. Following from the linear interference effects illustrated in Fig. 5, the EM_{LIN} term is negative throughout the entire stratosphere and most of the troposphere during days 1–22 for the Siberian case, while the westward-tilting structure of the waves indicates that the EM_{NL} term is again positive (see also Fig. 8d).

We note that the structure of $\Delta\langle Z^*\rangle$ in the Siberian case looks strikingly similar to that in the second period of the AM2 simulation; that is, the day 1–22 SGCM response is westward shifted, especially in the stratosphere, relative to the day 1–65 AM2 response. The phase of $\Delta\langle Z^*\rangle$ in the Siberian case in the SGCM shifts westward and out of phase with $\langle Z_c^*\rangle$ over the first few days of the run. This also occurs in AM2, albeit more quickly; however, unlike the AM2 case (Fig. 3), the SGCM wave response does not then shift eastward and in phase with $\langle Z_c^*\rangle$ (not shown). As is the case for other differences between the SGCM and AM2 simulations, it is not simple to explain why the transient ensemble-mean wave response differs so significantly between the two simulations (see section 4). But given the different wave responses, we now understand how differences in phasing between $\Delta\langle Z^*\rangle$ and $\langle Z_c^*\rangle$ exert correspondingly different linear interference effects on wave driving, and hence opposite sign NAM responses are obtained in the two simulations.

c. *Sensitivity to position and sign of the forcing in the SGCM*

To further probe the linear interference effect, we conduct 11 additional forcing simulations with the SGCM in which the forcing is shifted zonally at intervals of 30° longitude [i.e., λ_1 and λ_2 in (3) are increased in 30° increments; Table 1 simulations A–L]. For these experiments, this forcing should no longer be interpreted as an idealized snow forcing, but rather as a low-level cooling.

One of these additional simulations, a simulation with the forcing location given by $\lambda_1 = 150°$E and $\lambda_2 = 230°$E (henceforth the ''Pacific case,'' simulation E in Table 1),

illustrates the response to the forcing when the wave response constructively interferes with the control state wave. The wave response $\Delta\langle Z^*\rangle$ for this case is shown in Fig. 4c, and the $\Delta\langle Z\rangle$ response is shown in Fig. 4d. In this case, the all-wave spatial correlation between $\Delta\langle Z^*\rangle$ and $\langle Z_c^*\rangle$ is 0.58 and is determined by a very strong positive correlation in wave 1 of 0.96. This positive phasing of the wave fields translates into increased vertical wave activity propagation into the stratosphere. As in the cases discussed so far, EM_{LIN} dominates but unlike the Siberian case (simulation B), it is positive in the stratosphere. Correspondingly, wave activity is absorbed in the stratosphere, leading to a negative NAM response in the polar stratosphere, illustrated by the positive zonal-mean GPH response poleward of 60°N and above 10 hPa (Fig. 4d). While the coupling of the response into the troposphere for both cases is weak, the negative GPH response in the troposphere is weaker in the Pacific case (simulation E, Fig. 4d) than in the Siberian case (simulation B, Fig. 4b). Thus, the NAM signature of the Pacific case minus that of the Siberian case is consistently positive in the troposphere and stratosphere.

Figure 6 summarizes the results of the sensitivity study on the location of the forcing. Figure 6a shows that for the 12 sensitivity simulations, the polar-cap-averaged thickness response $\Delta\langle Z_t\rangle$ from 10 to 1 for days 10–40 is negatively correlated with the zonal-mean TOTAL E–P flux divergence response for a 40°–80°N and 10–1-hPa box for days 1–22 (variance explained: 88%).[1] We use the 10–1-hPa thickness response to highlight the changes in this layer, because it is in the mid-to-upper stratosphere where the response is most sensitive to the change in the forcing in the SGCM (as seen in Fig. 4). Figure 6b shows that the E–P flux divergence response is itself negatively correlated with the EM eddy heat flux response at 10 hPa $\Delta\{\langle v^*\rangle\langle T^*\rangle\}$ (variance explained: 81%). Thus, as expected, the total wave driving in the stratosphere is dominated by the vertical wave activity flux (Newman et al. 2001); this is, in turn, dominated by the EM term, as was found for the AM2 snow simulations. Figure 6c shows that the EM term (as in Fig. 6b) is, in turn, positively correlated with EM_{LIN} (variance explained: 98%). This correlation is close to perfect and points to the importance of linear regime dynamics in the interaction of surface forcings and the atmospheric circulation. Figure 6d shows that EM_{LIN} (as in Fig. 6c) is positively correlated with the anomaly correlation of $\Delta\langle Z^*\rangle$ and $\langle Z_c^*\rangle$ at 60°N for days 1–22 (as we calculated in Fig. 5; variance explained: 89%). This correlation reflects the wave 1 anomaly correlation, which explains roughly 86% of the variance in EM_{LIN}. Figure 6d also illustrates the relationship between forcing location (indicated by the labeled data points) and the wave 1 anomaly correlation. In general, forcing location is an excellent predictor of linear interference effects in the SGCM simulations.

We conclude that the phase of the wave 1 ensemble-mean response relative to the phase of the control state wave explains most of the wave driving response and hence the NAM response for this amplitude of forcing.

We may also test the role of phasing by switching the sign of the forcing; that is, by imposing a lower-tropospheric heating instead of a lower-tropospheric cooling in the SGCM. We choose the forcing centered at 70°E ($\lambda_1 = 30$°E and $\lambda_2 = 110$°E; simulation A in Table 1 and Fig. 6d) as the one for which we will switch the sign from a cooling to a heating; this simulation is simulation S in Table 1. In the cooling case, simulation A, the forcing generates a wave train that strongly destructively interferes with the control state wave: the all-wave and wave 1 $\Delta\langle Z^*\rangle - \langle Z_c^*\rangle$ anomaly correlations in this case are the most strongly negative in response to cooling among the 12 simulations, and a strong positive NAM response results (Figs. 7a,b). When we switch the sign of the forcing, we get an opposite-signed wave response that is in phase with $\langle Z_c^*\rangle$, generating strong constructive interference and a strong negative NAM response (Figs. 7c,d). The corresponding anomaly correlations for the all-wave, wave 1 and wave 2 eddy GPH fields are −0.71, −0.88, and 0.59 for the cooling and 0.59, 0.83, and −0.75 for the heating, respectively. While linear effects explain most of the responses, we note that there is some nonlinearity acting in the wave response: the anomaly correlations are not equal and opposite, and there is a slight but statistically significant eastward shift of the response wave in the heating case relative to the cooling case.

Collectively, these sensitivity simulations demonstrate the importance of the phasing of the wave response with the control state wave in generating a teleconnected response to a localized lower-tropospheric forcing. The high correlations between dynamical fields illustrated in Fig. 6 provide quantitative support for this feature of troposphere–stratosphere interaction.

d. Sensitivity to forcing strength in the SGCM

The dominance of EM_{LIN} in EM is contingent on the fact that the wave response generated by the forcing is relatively small. If we increase the magnitude of the forcing, we may enter a regime where the EM_{NL} term dominates. Starting with the standard Siberian case

[1] Although the decomposition TOTAL = EM + FL = EM_{LIN} + EM_{NL} + FL was derived above for the meridional eddy heat flux, the decomposition generalizes simply to the total E–P flux.

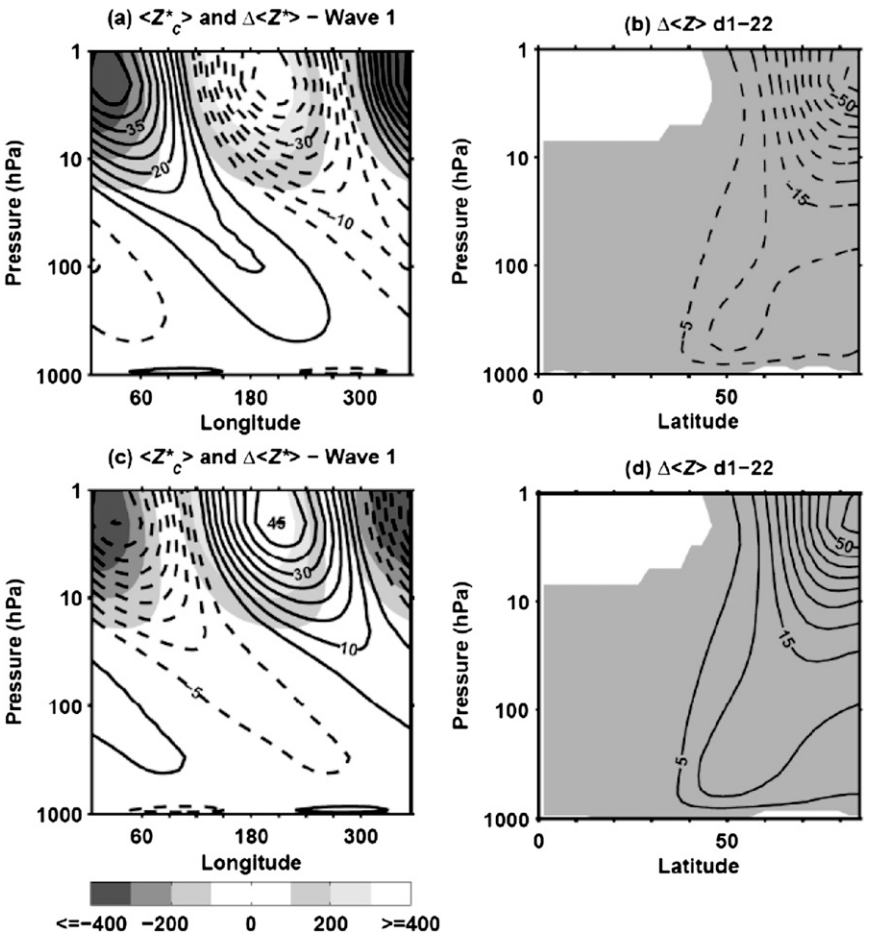

FIG. 7. (a),(c) As in Fig. 5b, but for simulations A and S, respectively. (b),(d) As in Fig. 4b, but for simulations A and S, respectively; gray shading shows 95% significance.

discussed in sections 2, 3b, and 3c, in which destructive interference is acting, we test the sensitivity to the strength of the forcing by decreasing and increasing Q_0 in (3) in the SGCM simulations. Figure 8 shows the response in polar-cap-averaged stratospheric thickness ($\Delta\langle Z_t\rangle$ from 10 to 1 hPa for days 10–40), the EM eddy heat flux response at 10 hPa averaged over 40°–80°N, the linear contribution EM_{LIN}, and the nonlinear contribution EM_{NL} as a function of forcing strength for seven simulations. The forcing strength has been normalized such that a forcing strength of 1 corresponds to the standard case previously discussed. Figure 8a shows, interestingly, that the circulation response is not monotonic in the strength of the forcing in this case, but in fact is a minimum at our standard forcing. This also holds true for the EM eddy heat flux response, although the minimum is weaker (Fig. 8b). The reason is that the linear response destructively interferes with the control state wave, so that the EM_{LIN} term is negative and decreases more or less linearly with the forcing (Fig. 8c), while the EM_{NL} term is consistently positive and increases more rapidly than linearly with the forcing (Fig. 8d). If the wave response is linear in the forcing, then we expect that that the EM_{LIN} and EM_{NL} terms should be linear and quadratic, respectively, in the forcing. Indeed, we find an excellent fit when a linear dependence on the forcing strength is fit to the EM_{LIN} term by linear regression (94% variance explained for a linear fit passing through the origin; solid curve in Fig. 8c) and a quadratic dependence on the forcing strength is fit to the EM_{NL} term, again by linear regression (99% variance explained for a quadratic fit passing through the origin; solid curve in Fig. 8d). The term EM_{NL} dominates EM once the forcing strength is sufficiently large, which occurs at roughly a doubling of the standard forcing strength.

4. Conclusions

In this study we have illustrated ways in which some of the complexities of the zonal-mean atmospheric

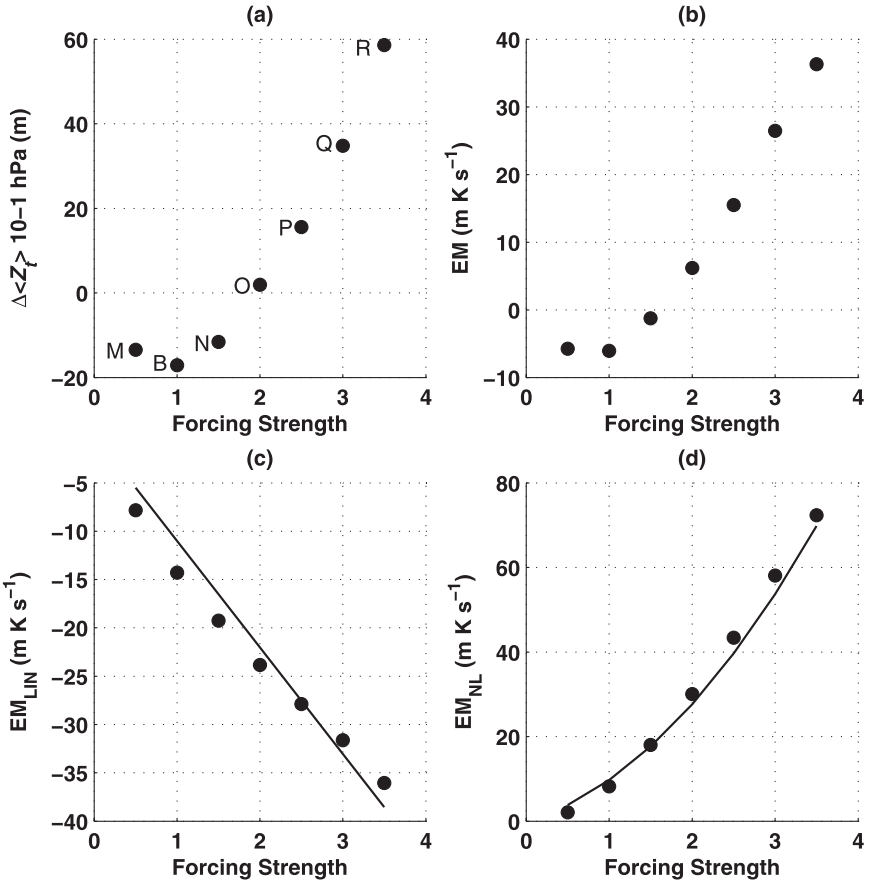

FIG. 8. Dependence of the SGCM response on forcing strength (simulations M, B, N–R in Table 1). (a) The 10–1-hPa $\Delta\langle Z_t\rangle$ and over days 10–40; (b) $\Delta\{\langle v^*\rangle\langle T^*\rangle\}$ (EM) at 10 hPa, averaged over 40°–80°N, and cumulative to day 22; (c) EM_{LIN}; and (d) EM_{NL}, as a function of forcing strength. The forcing strength has been normalized such that a forcing strength of 1 corresponds to the forcing discussed in section 2. The solid lines in (c) and (d) show the linear and quadratic fits passing through the origin, respectively.

circulation response to extratropical surface forcing can be explained using a linear interference analysis. Motivated by the observed connections between snow variability and annular mode anomalies, we have applied this analysis to comprehensive and simplified GCM simulations. Our major conclusion is that the effects of linear interference between the wave response and the control state wave, which is found by comparing wave phase and calculating spatial correlations, control the zonal-mean northern annular mode (NAM) response. The expectation is that linear interference effects dominate provided the wave response is small compared to the control state wave. To begin, we showed that the comprehensive GCM, GFDL AM2, exhibits a transient zonal-mean response that consists of an initial weak positive NAM tendency in the first 20 days, followed by a negative NAM tendency up to about day 65, and then terminating with a positive NAM tendency. At each stage, while the surface cooling consistently generates an upward-propagating Rossby wave train into the stratosphere, the extratropical stratospheric tendencies are driven by a wave activity anomaly that can be diagnosed in terms of the constructive or destructive interference of the planetary-scale wave response with the control state wave (Fig. 3). We have isolated this effect by decomposing the wave activity flux response into parts that are linear and nonlinear in the ensemble-mean wave response.

We then illustrated the linear interference effects more broadly by varying the location, strength, and sign of the forcing in the SGCM. In all simulations, the surface cooling consistently generates an upward-propagating Rossby wave (Figs. 1b,c and Figs. 4a,c, Figs. 7a,c, and Fig. 8d all highlight this point). The phasing of the wave response with the control state wave is the key determinant of the nature of the zonal-mean response to the

forcing (Fig. 1a and Figs. 4b,d). The interference effect, whether constructive or destructive, can be tuned by shifting the forcing location so that the response can become more or less phase matched with the control state wave.

In addition, we have shown that the importance of linear interference, and hence the zonal-mean extratropical response to this surface perturbation, depends on the forcing strength (Fig. 8). In nature, the magnitude of interannual lower-tropospheric diabatic heating anomalies can be relatively small, suggesting that linear interference is likely an important feature of externally forced troposphere–stratosphere interactions. It is important to note that as forcing strength increases, the shift into the nonlinear regime likely occurs at a weaker forcing strength in the SGCM than in nature because of the weak control state stationary waves in the SGCM. Nevertheless, it is interesting that our forcing, while somewhat larger than what may be found in nature, is not completely unrealistic in terms of the surface temperatures and magnitude of regional response, and that in the SGCM sensitivity study, we were close to the boundary of a regime where nonlinear effects came into play. Thus, we would expect that these considerations will be important in other modeling contexts where relatively strong forcings are used to elicit strong signals in the extratropics. But even this large-amplitude regime might be understood in a weakly nonlinear theoretical setting. For example, we find that the phase evolution of the ensemble-mean wave responses in the SGCM is not sensitive to the strength of the forcing during days 1–22 (not shown). This emphasizes that a transient linear model might provide accurate predictions of the NAM response to surface forcing.

In this setting, the role of the FL term in the time- and ensemble-mean eddy heat flux decomposition turns out to be minor. The FL term represents the ensemble-mean eddy fluxes driven by waves that are independent among realizations, typically high-frequency waves such as synoptic waves in the troposphere and stratospheric transients. We find that in this problem, the direct eddy heat flux response of such higher-frequency waves is of secondary importance to the NAM response. The minor role of FL represents a potential simplification of the linear dynamics needed to obtain the main features of the high-latitude zonal-mean response to surface forcing. This does not imply that high-frequency waves are unimportant in this class of problems. For example, high-frequency waves are indirectly involved in generating and maintaining low-frequency anomalies, such as the ensemble-mean wave response to surface forcing discussed in this study (Branstator 1992; Sobolowski et al. 2010).

By using the simplified GCM, we are able to generate large ensembles and to isolate dynamical mechanisms. Much of our motivation to study linear interference effects initially came from our experimentation with the simplified GCM, because the simplified GCM yielded a NAM response of opposite sign to what we expected (section 3b). As we have shown, the linear interference effect is also clearly operating in the comprehensive GCM simulations, but it first emerged most starkly in the simple GCM. This highlights the value of looking at examples across the model hierarchy (Held 2005) when trying to understand complex dynamics of the kind we are investigating here.

Nevertheless, the SGCM framework has its limitations. For example, it was difficult to compare the SGCM and AM2 simulations directly, because (i) the SGCM's control state wave is weaker and slightly eastward shifted relative to that of AM2, (ii) the transient evolution of the wave response is very different in the two models, (iii) stratosphere–troposphere interactions appear to be rather weak in the SGCM, and (iv) the NAM response in the SGCM simulations was not statistically significant beyond days 20–30. We have not been able to explain many aspects of the discrepancies of the response in the two models, despite the fact that the linear interference effects are at work in both frameworks. Our results suggest that linear modeling approaches will be useful in helping constrain some aspects of the extratropical response problem.

Acknowledgments. We acknowledge the support of the Natural Sciences and Engineering Research Council of Canada postgraduate scholarship and Discovery Grant, the Canadian Foundation for Climate and Atmospheric Sciences Grant 506, and the Canadian International Polar Year Cryosphere Network. The authors would also like to acknowledge and thank the two reviewers for their constructive comments and suggestions.

REFERENCES

Anderson, J., and Coauthors, 2004: The new GFDL global atmosphere and land model AM2–LM2: Evaluation with prescribed SST simulations. *J. Climate,* **17,** 4641–4673.

Baldwin, M. P., and T. P. Dunkerton, 2001: Stratospheric harbingers of anomalous weather regimes. *Science,* **294,** 581–584.

——, and D. W. J. Thompson, 2009: A critical comparison of stratosphere-troposphere coupling indices. *Quart. J. Roy. Meteor. Soc.,* **135,** 1661–1672.

——, D. B. Stephenson, D. W. J. Thompson, T. J. Dunkerton, A. J. Charlton, and A. O'Neill, 2003: Stratospheric memory and extended-range weather forecasts. *Science,* **301,** 636–640.

Branstator, G., 1992: The maintenance of low-frequency atmospheric anomalies. *J. Atmos. Sci.,* **49,** 1924–1945.

Brown, R. D., and P. Mote, 2009: The response of Northern Hemisphere snow cover to a changing climate. *J. Climate,* **22,** 2124–2145.

Chan, C. J., and R. A. Plumb, 2009: The response of the troposphere to stratospheric perturbations and its dependence on the state of the troposphere. *J. Atmos. Sci.,* **66,** 2107–2115.

Cohen, J., and D. Rind, 1991: The effect of snow cover on the climate. *J. Climate,* **4,** 689–706.

——, and D. Entekhabi, 1999: Eurasian snow cover variability and Northern Hemisphere climate predictability. *Geophys. Res. Lett.,* **26,** 345–348.

——, M. Barlow, P. Kushner, and K. Saito, 2007: Stratosphere–troposphere coupling and links with Eurasian land-surface variability. *J. Climate,* **21,** 5335–5343.

Czaja, A., and C. Frankignoul, 2002: Observed impact of Atlantic SST anomalies on the North Atlantic oscillation. *J. Climate,* **15,** 606–623.

DeWeaver, E., and S. Nigam, 2004: On the forcing of ENSO teleconnections by anomalous heating and cooling. *J. Climate,* **17,** 3225–3235.

Fletcher, C. G., and P. J. Kushner, 2011: The role of linear interference in the annular mode response to tropical SST forcing. *J. Climate,* in press.

——, ——, and J. Cohen, 2007: Stratospheric control of the extratropical circulation response to surface forcing. *Geophys. Res. Lett.,* **34,** L21802, doi:10.1029/2007GL031626.

——, S. C. Hardiman, P. J. Kushner, and J. Cohen, 2009a: The dynamical response to snow cover perturbations in a large ensemble of atmospheric GCM integrations. *J. Climate,* **22,** 1208–1222.

——, P. J. Kushner, A. Hall, and X. Qu, 2009b: Circulation responses to snow albedo feedback in climate change. *Geophys. Res. Lett.,* **36,** L09702, doi:10.1029/2009GL038011.

Garfinkel, C. I., and D. L. Hartmann, 2008: Different ENSO teleconnections and their effects on the stratospheric polar vortex. *J. Geophys. Res.,* **113,** D18114, doi:10.1029/2008JD009920.

——, ——, and F. Sassi, 2010: Tropospheric precursors of anomalous Northern Hemisphere stratospheric polar vortices. *J. Climate,* **23,** 3282–3299.

Gerber, E. P., and L. M. Polvani, 2009: Stratosphere–troposphere coupling in a relatively simple AGCM: The importance of stratospheric variability. *J. Climate,* **22,** 1920–1933.

——, ——, and D. Ancukiewicz, 2008a: Annular mode time scales in the Intergovernmental Panel on Climate Change Fourth Assessment Report models. *Geophys. Res. Lett.,* **35,** L22707, doi:10.1029/2008GL035712.

——, S. Voronin, and L. M. Polvani, 2008b: Testing the annular mode autocorrelation time scale in simple atmospheric general circulation models. *Mon. Wea. Rev.,* **136,** 1523–1536.

Gong, G., D. Entekhabi, and J. Cohen, 2002: A large-ensemble model study of the wintertime AO–NAO and the role of interannual snow perturbations. *J. Climate,* **15,** 3488–3499.

——, ——, and ——, 2003: Modeled Northern Hemisphere winter climate response to realistic Siberian snow anomalies. *J. Climate,* **16,** 3917–3931.

Groisman, P. Y., T. R. Karl, and R. W. Knight, 1994: Changes of snow cover, temperature, and radiative heat balance. *J. Climate,* **7,** 1633–1656.

Hardiman, S. C., P. J. Kushner, and J. Cohen, 2008: Investigating the ability of general circulation models to capture the effects of Eurasian snow cover on winter. *J. Geophys. Res.,* **113,** D21123, doi:10.1029/2008JD010623.

Held, I. M., 2005: The gap between simulation and understanding in climate modeling. *Bull. Amer. Meteor. Soc.,* **86,** 1609–1614.

——, and M. J. Suarez, 1994: A proposal for the intercomparison of the dynamical cores of atmospheric general circulation models. *Bull. Amer. Meteor. Soc.,* **75,** 1825–1830.

Henderson, G. R., and D. J. Leathers, 2009: European snow cover extent variability and associations with atmospheric forcings. *Int. J. Climatol.,* **30,** 1440–1451, doi:10.1002/joc.1990.

Ineson, S., and A. A. Scaife, 2009: The role of the stratosphere in the European response to El Niño. *Nat. Geosci.,* **2,** 32–36, doi:10.1038/NGEO381.

Kushner, P. J., and L. M. Polvani, 2004: Stratosphere–troposphere coupling in a relatively simple AGCM: The role of eddies. *J. Climate,* **17,** 629–639.

Kushnir, Y., W. A. Robinson, P. Chang, and A. W. Robertson, 2006: The physical basis for predicting Atlantic sector seasonal-to-interannual climate variability. *J. Climate,* **19,** 5949–5970.

Limpasuvan, V., and D. L. Hartmann, 2000: Wave-maintained annular modes of climate variability. *J. Climate,* **13,** 4414–4429.

Martius, O., L. M. Polvani, and H. C. Davies, 2009: Blocking precursors to stratospheric sudden warming events. *Geophys. Res. Lett.,* **36,** L14806, doi:10.1029/2009GL038776.

McDaniel, B. A., and R. X. Black, 2005: Intraseasonal dynamical evolution of the northern annular mode. *J. Climate,* **18,** 3820–3839.

Newman, P. A., E. R. Nash, and J. E. Rosenfield, 2001: What controls the temperature of the Arctic stratosphere during the spring? *J. Geophys. Res.,* **106** (D17), 19 999–20 010.

Polvani, L. M., and P. J. Kushner, 2002: Tropospheric response to stratospheric perturbations in a relatively simple general circulation model. *Geophys. Res. Lett.,* **29,** 1114, doi:10.1029/2001GL014284.

——, and D. W. Waugh, 2004: Upward wave activity flux as precursor to extreme stratospheric events and subsequent anomalous surface weather regimes. *J. Climate,* **17,** 3548–3554.

Reichler, T., P. J. Kushner, and L. M. Polvani, 2005: The coupled stratosphere–troposphere response to impulsive forcing from the troposphere. *J. Atmos. Sci.,* **62,** 3337–3352.

Robinson, W. A., 2000: Review of WETS—The Workshop on Extra-Tropical SST anomalies. *Bull. Amer. Meteor. Soc.,* **81,** 567–577.

Sobolowski, S., G. Gong, and M. Ting, 2010: Modeled climate state and dynamic responses to anomalous North American snow cover. *J. Climate,* **23,** 785–799.

Thompson, D. W. J., and J. M. Wallace, 1998: The Arctic Oscillation signature in the wintertime geopotential height and temperature fields. *Geophys. Res. Lett.,* **25,** 1297–1300.

——, and ——, 2000: Annular modes in the extratropical circulation. Part I: Month-to-month variability. *J. Climate,* **13,** 1000–1016.

Vavrus, S., 2007: The role of terrestrial snow cover in the climate system. *Climate Dyn.,* **29,** 73–88.